ANALYTICAL SCIENCES OCTOBER 2002, VOL. 18

Laser Ablation Inductively Coupled Plasma Mass Spectrometry (LA-ICP-MS): Comparison of Different Internal Standardization Methods Using Laser-induced Plasma (LIP) Emission and LA-ICP-MS Signals

Masaki OHATA, Hiroyuki YASUDA, Yoshimichi NAMAI, and Naoki FURUTA†

Faculty of Science and Engineering, Department of Applied Chemistry, Chuo University, 1-13-27, Kasuga, Bunkyo-ku, Tokyo 112–8551, Japan

The source of signal variations that governs the analytical performance of laser ablation inductively coupled plasma mass spectrometry (LA-ICP-MS) was investigated in this study. In order to specify the source of signal variations of LA-ICP-MS, laser-induced plasma (LIP) Fe emission, LA-ICP-MS Fe^+ and LA-ICP-MS Ni^+ signals were used as internal standards for the determination of trace elements in low-alloy steel certified reference materials (BS 50D and JSS 1005-1008). Fe I 373.5 nm emission signals from LIP were measured, while trace element LA-ICP-MS signals were collected. After that, the LIP emission signals, LA-ICP-MS Fe^+ and LA-ICP-MS Ni^+ signals were used as internal standards, and the analytical performance was evaluated by the RSDs and the correlation coefficients (r) of the calibration curves. The improvement factors were dependent on the internal standardization methods. Analytical precisions (RSDs) of trace element LA-ICP-MS signals were improved by factors of 1.5 – 3.3 using LIP Fe emission signals as an internal standard. The improvement factors of 2.5 – 5.9 and 4.1 – 17 were obtained by using LA-ICP-MS Fe^+ and LA-ICP-MS Ni^+ signals as internal standards, respectively. Better correlation coefficients (r) were also obtained using the LA-ICP-MS signal compensation (0.9985 by LA-ICP-MS Fe^+ and 0.9996 by LA-ICP-MS Ni^+) rather than the LIP Fe emission compensation (0.9932). In this paper we compare and discuss the analytical performance achieved by LA-ICP-MS using LIP Fe emission, LA-ICP-MS Fe^+ and LA-ICP-MS Ni^+ signals as internal standards.

(Received May 2, 2002; Accepted August 26, 2002)

Introduction

Laser ablation (LA) coupled with ICP-AES (LA-ICP-AES)[1-11] and ICP-MS (LA-ICP-MS)[11–29] has become a popular method for the determination of trace elements in solid samples. There are numerous advantages of LA-ICP-AES/MS for direct solid sample analysis: for example, sample preparation is minimum, loss of volatile analytes is avoided, contamination from reagents is reduced and sample throughput is increased. Furthermore, LA can also be used to analyze refractory solid samples. Moreover, spatial distribution analysis can be conducted with a resolution of less than 10 μm. However, there are some disadvantages with LA-ICP-MS. In general, the precision and accuracy of LA-ICP-MS are worse than those of ICP-MS with conventional pneumatic nebulization. One of the reasons for this poorer analytical performance is the large variation of the ablated amount owing to fluctuations in laser power on a shot-to-shot basis, heterogeneous chemical and textural compositions, different sample surface characteristics and vaporization characteristics. Several methods have been proposed to improve the analytical performance of LA-ICP-AES/MS. Calibration with matrix matched standards and internal standardization using elements in the samples have been used widely.[3,5,6,8,9,15,16,20,24] Monitoring acoustic waves produced during laser ablation,[1,2,7,10] emission signals from laser-induced plasma (LIP)[4] that can be observed on the surface of the sample, scattered light during sample transport,[12,13,17] and shot to shot normalization[23] have been reported. The purpose of this study is to elucidate the source of signal variations that governs the analytical performance of LA-ICP-MS. In this study we compensated for the variations of LA-ICP-MS signals for the determination of Ti, V, Cr, Co, Ni, Cu, Zr, Nb, Mo, and W in Fe low-alloy steel reference materials. We selected the laser-induced plasma (LIP) emission signal as an internal standard because it can be considered that the analytical performance of LA-ICP-MS is determined inside the sample cell during laser ablation. The LIP Fe I 373.5 nm emission signals observed on the surface of the low-alloy steel reference materials during laser ablation were used as an internal standard to correct for the signal variations detected by LA-ICP-MS. Internal standardizations using $^{57}Fe^+$ and $^{60}Ni^+$ ion signals detected by LA-ICP-MS were also conducted and compared to the LIP Fe emission standardization. From these observed results, we discussed and specified the sources of signal variations of LA-ICP-MS.

Experimental

Figure 1 shows schematic diagram of the instrument configuration. Operating conditions of the laser-induced plasma atomic emission spectrometer (LIP-AES) and ICP-MS are listed in Table 1. The carriage system consists of two parallel

† To whom correspondence should be addressed.
E-mail: nfuruta@chem.chuo-u.ac.jp

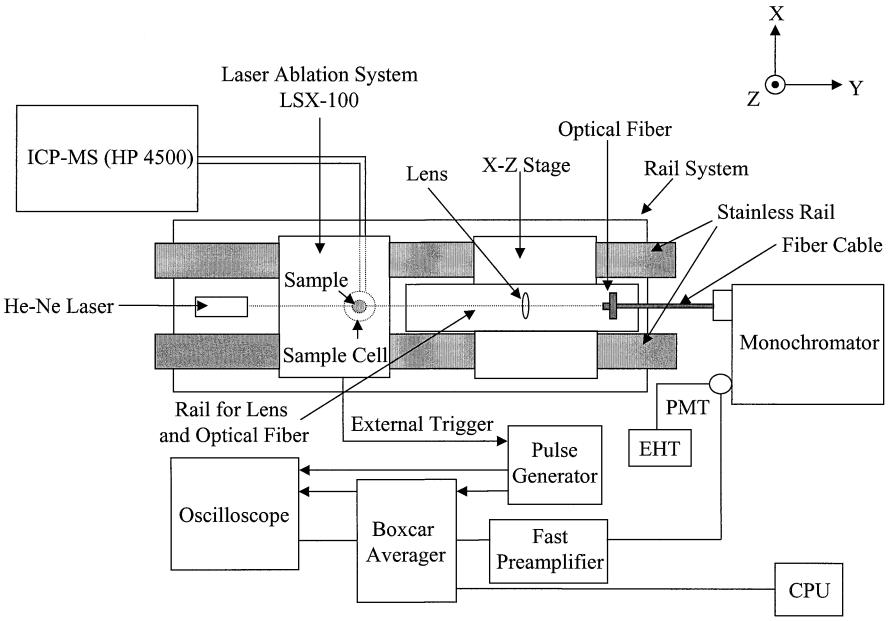

Fig. 1 Schematic diagram of the instrument configuration used for measuring laser-induced plasma (LIP) emission and LA-ICP-MS signals.

cylindrical stainless-steel rails, whose horizontal position can be adjusted accurately. An LSX-100 Nd:YAG laser ablation instrument (CETAC, Omaha, Nebraska, USA) was installed on the rail system. The LSX-100 employs a specially designed TEM_{00} UV Nd:YAG 266 nm laser, a Gaussian beam profile, and can be operated at a repetition rate of 20 Hz. In this study, both Fe emission signals from the LIP and LA-ICP-MS trace element signals were measured simultaneously. Because the LIP can be observed on the sample surface during the laser ablation, a quartz sample cell (45 cm^3) was laboratory-made for the ablation cell to detect the UV emission signals from the LIP. An X-Z stage was used to collect emission signals from the LIP. For collection of LIP Fe emission signals, an optical lens (45 mm diameter and 170 mm of focal length) and an optical fiber (0.8 mm of core diameter, Mitsubishi Cable Industries, Ltd., Japan) were installed on the X-Z stage. A He-Ne laser was also located on the rail system for accurate parallel and horizontal alignment of the optical lens and the optical fiber. The optical lens was located on the X-Z stage and the LIP was imaged down by a factor of 2. Since the core diameter of the optical fiber was 0.8 mm, emission signals that were measured from the LIP corresponded to a 1.6 mm diameter area. LIP emission signals collected by the optical fiber were dispersed by a scanning monochromator (HR 1000, Jobin Yvon-Horiba, France). Signals were detected using a photomultiplier tube (PMT) (R919, Hamamatsu Photonics, Hamamatsu, Japan). Signals detected by the PMT were introduced into a fast preamplifier (Model SR 240, Stanford Research Systems, California, USA), and converted from current to voltage, and amplified. The amplified voltage was sampled by a boxcar averager (Model SR 250, Stanford Research Systems, California, USA), which enabled the signals to integrate. LIP emission signals were also monitored by an oscilloscope (TDS 360, Tektronix Inc., Beaverton, Oregon, USA). In this study, the output energy (2.1 ± 0.1 mJ) and frequency (20 Hz) of the laser were fixed and operated for 30 s, *i.e.*, 600 laser shots were conducted for all measurements. The laser was focused on the sample surface for each laser ablation (a raster mode) thus the power density was kept constant during 30 s laser ablation. Pre-ablation was also performed to clean the sample surface. The refraction effect at the curved surface of the cylindrical quartz cell was avoided by maintaining the position of the *x*- and *z*-axes constant during all experiments, *i.e.*, the sample cell was only moved along the *y*-axis for 5 measurements of each Fe low-alloy steel.

An external trigger, which triggered the system when laser ablation started, was introduced into a digital pulse generator (Model DG 535, Stanford Research Systems, California, USA). A 250 ns delay from the external trigger was set by the digital pulse generator (1st pulse) to set 0 ns of LIP Fe emission signals displayed on the oscilloscope, as shown in Fig. 2. In addition, a delay time of 170 ns from the 1st pulse was set by the digital pulse generator (2nd pulse) to start the sampling gate of the boxcar averager. The sampling gate width was determined by monitoring the LIP Fe I 373.5 nm emission signals displayed on the oscilloscope. A sampling gate width of 4000 ns was selected, because this sampling gate width integrated all LIP Fe emission signals. The LIP 373.0 nm emission signal is also shown in Fig. 2 as a background. LIP Fe and background emission signals were integrated and accumulated by a boxcar averager during 30 s laser ablation. LIP background emission signals that accumulated were subtracted from LIP Fe emission signals accumulated, and the resultant signals were used as an internal standard to compensate for the variations of trace element LA-ICP-MS signals.

Certified low-alloy steel disk standards (BS 50D, Brammer Standard Company, Inc., TX, USA and JSS 1005-1008, The Iron and Steel Institute of Japan, Tokyo, Japan) were used. Certified and reference values for the trace elements of interest are listed in Table 2. Iron is a major element in these low-alloy steel CRMs. The isotopes of ^{47}Ti, ^{51}V, ^{53}Cr, ^{59}Co, ^{60}Ni, ^{63}Cu, ^{90}Zr, ^{93}Nb, ^{95}Mo, ^{182}W and ^{57}Fe were measured by LA-ICP-MS. The ICP-MS used in this study was HP 4500 (Yokogawa Analytical Systems, Tokyo, Japan). Ion signals were observed with time resolved analysis for 60 s using the instrument software. Ablated particles were transported to the ICP using a tygon tube (1/16 inch i.d., 2 m length).

Table 1 Operating conditions for LIP-AES and ICP-MS

LIP-AES	
Laser ablation system	LSX-100 (Cetac)
Laser	Nd:YAG
Laser mode	Q-switched
Wavelength	266 nm
Pulse duration	8 ns
Energy	2.1 ± 0.1 mJ
Frequency	20 Hz
Ablation time	30 s
Monochromator	HR-1000 (Jobin Yvon)
Focal length	1000 mm
Grating	2400 grooves mm^{-1}
Height of entrance and exit slits	7 mm
Width of entrance and exit slits	50 μm
Pulse generator	Model DG 535 (Stanford Research Systems)
Optical fiber	(Mitsubishi Cable Industries)
Diameter	800 μm
Detector	
Photomultiplier tube	R 919 (Hamamatsu Photonics)
High voltage power supply	Model PS 325 (Stanford Systems, Inc.)
Voltage	–580 V
Fast preamplifier	Model SR 240 (Stanford Research Systems)
Boxcar averager	Model SR 250 (Stanford Research Systems)
Gate width	4000 ns
Integration time	1 s
Measurement time	30 s
Oscilloscope	TDS 360 (Tektronix)
ICP-MS	HP4500 (Yokogawa Analytical Systems)
Incident power	1.3 kW
Plasma gas flow rate	15.0 l min^{-1}
Auxiliary gas flow rate	1.0 l min^{-1}
Carrier gas flow rate	1.5 l min^{-1}
Analysis mode	Time resolved analysis
Acquisition	Single point, peak hopping
Integration time per point	10 ms
Measurement time	60 s
Isotopes and elements measured	^{47}Ti, ^{51}V, ^{53}Cr, ^{57}Fe, ^{59}Co, ^{60}Ni, ^{63}Cu, ^{90}Zr, ^{93}Nb, ^{95}Mo, ^{182}W

Results and Discussion

Comparison of analytical precision using LIP Fe emission, LA-ICP-MS Fe^+ and LA-ICP-MS Ni^+ signals as internal standards

Analytical precisions (RSDs) of LA-ICP-MS obtained with LIP Fe emission, LA-ICP-MS Fe^+ and LA-ICP-MS Ni^+ signals compensations were compared to those obtained without compensations. In general, RSDs with internal standardizations were much more improved than those without corrections, with exception of Ti and Zr, as shown in Fig. 3. Except for Ti and Zr, RSDs without internal standardization were about 10 – 20% for each element. Figure 4 shows RSDs obtained with and without different compensations as a function of number of ion counts detected by LA-ICP-MS, excluding Ti and Zr. In general, it can be seen that RSDs decreased with increase in number of ion counts. The curves fitted for different compensations are also indicated in Fig. 4. From the slope of the fitted curves, the compensation degrees can be figured out.

Table 2 Certified values (%) in low-alloy steel standards

	BS 50D	JSS 1005	JSS 1006	JSS 1007	JSS 1008
Ti	0.0001	0.004	0.005	0.021	0.052
V	0.0004	0.005	0.01	0.03	0.06
Cr	0.0003	0.007	0.013	0.053	0.102
Co	0.0026	0.009	0.014	0.035	0.065
Ni	0.0012	0.009	0.014	0.054	0.103
Cu	0.0004	0.005	0.01	0.049	0.099
Zr	< 0.0002[a]	0.006	0.003[a]	0.002[a]	0.011
Nb	0.0002	0.004	0.009	0.03	0.06
Mo	0.00004[a]	0.005	0.01	0.03	0.062
W	0.0002[a]	0.006[a]	0.01	0.03	0.058

a. Reference values.

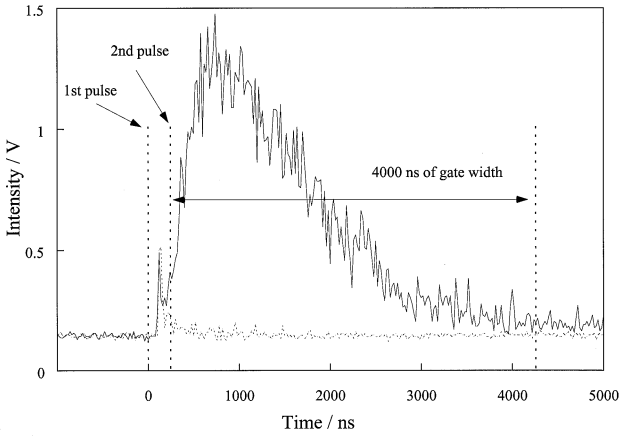

Fig. 2 Time resolved LIP Fe I 373.5 nm and 373.0 nm background signals observed on an oscilloscope. Measurements were conducted by using a photomultiplier tube operated at –580 V. The dotted lines (– – –) indicate the first and the second pulses generated by the digital pulse generator and the end of the sampling gate width of 4000 ns determined by the boxcar averager. The solid line (——) indicates LIP Fe I 373.5 nm emission signal. The fine dotted line (·····) indicates LIP 373.0 nm emission signal as a background.

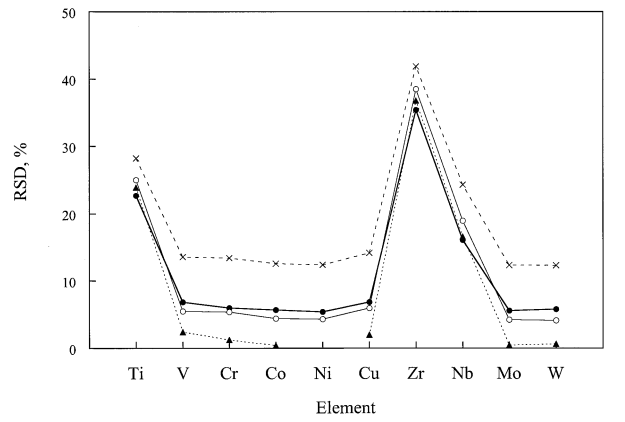

Fig. 3 Relative standard deviations (RSDs) obtained with and without compensation methods. Five measurements were repeated for JSS 1005. -×-: without correction, —●—: with LIP Fe emission correction, —○—: with LA-ICP-MS Fe^+ correction, and -▲-: with LA-ICP-MS Ni^+ correction.

The steeper the fitted curve is, the larger the compensation degree is. From the fitted curves, it can be evaluated that the

Table 3 RSD improvement factors (RSD without correction/RSD with correction) obtained by different compensation methods

	BS 50D			JSS1005			JSS1006			JSS1007			JSS1008		
	LIP Fe	LA-ICP-MS Fe^+	LA-ICP-MS Ni^+	LIP Fe	LA-ICP-MS Fe^+	LA-ICP-MS Ni^+	LIP Fe	LA-ICP-MS Fe^+	LA-ICP-MS Ni^+	LIP Fe	LA-ICP-MS Fe^+	LA-ICP-MS Ni^+	LIP Fe	LA-ICP-MS Fe^+	LA-ICP-MS Ni^+
^{47}Ti	1.1	1.1	1.0	1.2	1.1	1.2	0.81	0.79	0.71	1.9	2.1	3.8	2.0	4.2	4.9
^{51}V	1.3	1.6	2.0	2.0	2.5	5.6	3.9	3.2	19	2.4	3.4	22	2.3	7.1	10
^{53}Cr	1.8	2.9	4.5	2.2	2.5	11	3.0	2.7	9.5	2.3	3.2	13	2.5	7.3	15
^{59}Co	1.7	3.5	6.7	2.2	2.8	31	3.1	2.8	10	2.3	2.8	14	3.4	5.2	8.5
^{60}Ni	1.7	4.4	—	2.3	2.9	—	4.0	3.1	—	2.5	3.1	—	2.8	8.4	—
^{63}Cu	1.3	2.2	3.2	2.1	2.4	7.1	2.8	2.3	6.0	2.4	2.4	6.6	4.6	3.0	3.8
^{90}Zr	1.0	1.0	1.0	1.2	1.1	1.1	0.93	0.93	0.89	1.3	1.1	1.2	3.0	1.9	2.1
^{93}Nb	1.4	1.7	2.0	1.5	1.3	1.5	2.6	2.2	1.9	2.5	3.1	15	2.5	7.3	13
^{95}Mo	1.1	1.4	1.6	2.2	2.9	27	3.4	3.1	9.8	2.5	3.0	36	3.8	4.5	6.6
^{182}W	1.8	3.6	9.0	2.1	3.0	20	3.8	3.0	19	2.8	2.7	11	3.9	4.2	6.1
Ave.[a]	1.5	2.7	4.1	2.1	2.5	15	3.3	2.8	11	2.5	3.0	17	3.2	5.9	9.1

a. Averaged values for elements excluding Ti and Zr.

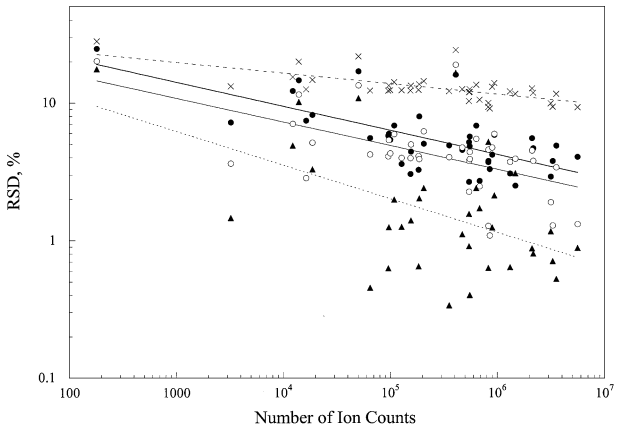

Fig. 4 RSDs of elements obtained by different compensation methods as a function of number of ion counts. -×-: without correction, —●—: with LIP Fe emission correction, —○—: with LA-ICP-MS Fe^+ correction, and -▲-: with LA-ICP-MS Ni^+ correction.

Table 4 Correlation coefficients (r) obtained with and without corrections

	Without correction	LIP Fe	LA-ICP-MS Fe^+	LA-ICP-MS Ni^+
Ti	0.9906	0.9937	0.9981	0.9992
V	0.9904	0.9941	0.9990	0.9999
Cr	0.9914	0.9951	0.9993	1.0000
Co	0.9918	0.9954	0.9995	1.0000
Ni	0.9926	0.9959	0.9996	—
Cu	0.9909	0.9946	0.9990	0.9999
Zr	0.9918	0.9904	0.9925	0.9890
Nb	0.9865	0.9909	0.9975	0.9991
Mo	0.9857	0.9905	0.9973	0.9991
W	0.9844	0.9894	0.9970	0.9990
Ave.[a]	0.9892	0.9932	0.9985	0.9996

a. Averaged values for elements excluding Ti and Zr.

compensation degrees of RSDs increased with increase in number of ion counts. More than 10^5 ion counts showed that the effective compensation as RSDs were improved to less than 10% for all internal standardizations. All of the RSD improvement factors (RSD without correction/RSD with correction) obtained by different compensation methods are listed in Table 3. Zirconium variations were not compensated by any of the internal standardization methods. Titanium variations also were not compensated when Ti concentrations were low (BS 50D, JSS 1005 and 1006). The fact that Zr and Ti show the different behavior compared with other elements can be considered to be because Zr and Ti remain as refractory particles inside both the laser ablation cell and the ICP. From the averaged values excluding Ti and Zr, several interesting trends can be observed. The improvement factors by LIP Fe emission signals (1.5 – 3.3) were worse than those of LA-ICP-MS Fe^+ signals (2.5 – 5.9) and LA-ICP-MS Ni^+ signals (4.1 – 17). Improvement factors obtained by LA-ICP-MS Ni^+ signals were better than those obtained by the other two compensation methods. The reason why the improvement factors obtained by LA-ICP-MS Ni^+ signals were better than those obtained by LA-ICP-MS Fe^+ signals may be the big difference of number of ions between major Fe and other trace elements in the Fe low-alloy steels. Such big differences may cause the different behavior for Fe and for other elements in a mass spectrometer due to a space charge effect.

Comparison of accuracy using LIP Fe emission, LA-ICP-MS Fe^+ and LA-ICP-MS Ni^+ signals as internal standards

The accuracy of LA-ICP-MS was also evaluated using various methods of compensation. Table 4 lists correlation coefficients (r) of the calibration curves prepared by ablating the Fe low-alloy steel CRMs (BS 50D and JSS 1005-1008). The certified and reference values listed in Table 2 were used to make calibration curves and to calculate the correlation coefficients (r). With the exception of Zr, correlation coefficients were improved using different signal compensations. The correlation coefficients (r) using LA-ICP-MS Fe^+ and LA-ICP-MS Ni^+ signals compensations (0.9985 and 0.9996, respectively) were better than those obtained by LIP Fe emission correction (0.9932). It should be noted that the best fits were obtained using LA-ICP-MS Ni^+ signals as an internal standard, which varied from 0.9990 to 1.0000 with exception of Zr. The relative deviation (%) was calculated as follows: the difference between the analytical result obtained using the calibration curve and the certified or reference value was divided by the certified or reference value ([(measured value – certified value)/certified value] × 100 (%)). Figure 5 shows the relative deviations (%) obtained with and without different compensation methods as a function of number of ion counts excluding Ti and Zr. The

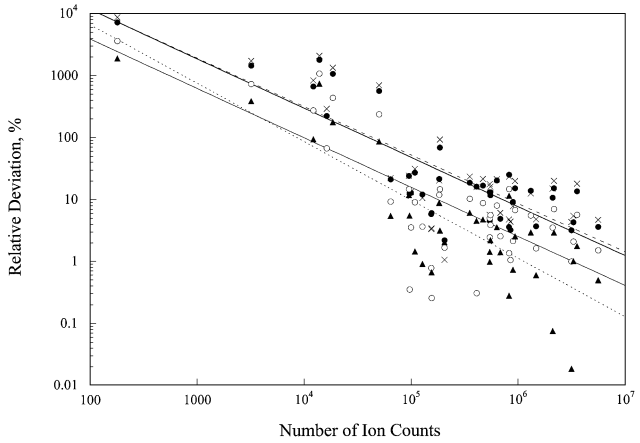

Fig. 5 Relative deviations (%) of elements obtained by different compensation methods as a function of number of ion counts. -×-: without correction, —●—: with LIP Fe emission correction, —○—: with LA-ICP-MS Fe^+ correction, and -▲-: with LA-ICP-MS Ni^+ correction.

relative deviations (%) decreased with increase in number of ion counts. Moreover, from the fitted curve, it can be evaluated that the compensation degrees of the relative deviations also increased with increase in number of ion counts.

Conclusions

For Fe low-alloy steels, LIP Fe emission and LA-ICP-MS Fe^+ and LA-ICP-MS Ni^+ signals have been used as internal standards to compensate for the signal variations in the laser ablation cell, the transportation system, and the ICP-MS spectrometer. Excluding Ti and Zr, it can be concluded that the variations of LA-ICP-MS signals of trace elements in these low-alloy steels were significantly compensated for using LIP emission and LA-ICP-MS signals as internal standards. In general, the improvement factors were large with increase in number of ion counts of LA-ICP-MS. The analytical precision (RSD) with LIP Fe emission compensation was improved by factors of 1.5 – 3.3 compared to that without correction. Better RSD improvement factors were, however, obtained using LA-ICP-MS Fe^+ signals (2.5 – 5.9) and LA-ICP-MS Ni^+ signals (4.1 – 17) as internal standards for trace element determination. The correlation coefficients (r) using LA-ICP-MS Fe^+ and LA-ICP-MS Ni^+ signal compensations (0.9985 and 0.9996, respectively) were better than those obtained by LIP Fe emission correction (0.9932). Based on the assumption that the variations of LIP Fe emission signals reflect fluctuations in the ablation cell during laser ablation, it can be concluded that the variation in the ablation cell makes a relatively small contribution to the total source of variation of LA-ICP-MS. These results imply that another source of variations of the LA-ICP-MS exists in the transportation system and the ICP-MS spectrometer. As the variations of LA-ICP-MS Fe^+ and LA-ICP-MS Ni^+ signals reflect the sum of the variations that occur in the laser ablation cell, the transportation system, and the ICP-MS spectrometer, the RSD and the accuracy are improved because of the correlative relation between LA-ICP-MS Fe^+ and LA-ICP-MS Ni^+ signals and trace element LA-ICP-MS signals. The variations of Ti and Zr were not compensated by any of the internal standardization methods. Ti and Zr can be considered to remain as refractory particles inside both of the laser ablation cell and the ICP, so they did not show the same fluctuation signals as other trace elements in low-alloy steel samples.

Acknowledgements

The authors would like to acknowledge Dr. Isacc. B. Brenner (Environmental Analytical Laboratory, Analytical Laboratory, Ben-Gurion University of Negev) for his constructive and invaluable comments.

References

1. G. Chen and E. S. Yeung, *Anal. Chem*., **1988**, *60*, 2258.
2. H. Pang, D. R. Wiederin, R. S. Houk, and E. S. Yeung, *Anal. Chem*., **1991**, *63*, 390.
3. N. Furuta, *Appl. Spectrosc*., **1991**, *45*, 1372.
4. A. Fernandez, X. L. Mao, W. T. Chan, M. A. Shannon, and R. E. Russo, *Anal. Chem*., **1995**, *67*, 2444.
5. V. Kanicky, V. Otruba, and J. M. Mermet, *Appl. Spectrosc*., **1998**, *52*, 638.
6. V. Kanicky and J. M. Mermet, *Fresenius' J. Anal. Chem*., **1999**, *363*, 294.
7. V. Kanicky, V. Otruba, and J. M. Mermet, *Fresenius' J. Anal. Chem*., **1999**, *363*, 339.
8. J. Nolte, F. Scheffler, S. Mann, and M. Paul, *J. Anal. At. Spectrom*., **1999**, *14*, 597.
9. M. M. Heino, O. F. X. Donard, and J. M. Mermet, *J. Anal. At. Spectrom*., **1999**, *14*, 675.
10. V. Kanicky, V. Otruba, and J. M. Mermet, *Fresenius' J. Anal. Chem*., **2000**, *366*, 228.
11. J. D. Winefordner, I. B. Gornushkin, D. Pappas, O. I. Matveev, and B. W. Smith, *J. Anal. At. Spectrom*., **2000**, *15*, 1161.
12. T. Tanaka, K. Yamamoto, T. Nomizu, and H. Kawaguchi, *Anal. Sci*., **1995**, *11*, 967.
13. S. A. Baker, B. W. Smith, and J. D. Winefordner, *Appl. Spectrosc*., **1998**, *52*, 154.
14. H. F. Falk, B. Hattendorf, K. Krengel-Rothensee, N. Wieberneit, and D. L. Dannen, *Fresenius' J. Anal. Chem*., **1998**, *362*, 468.
15. D. Gunter, A. Audetat, R. Frischknecht, and C. A. Heirich, *J. Anal. At. Spectrom*., **1998**, *13*, 263.
16. S. Shuttleworth and D. T. Kremser, *J. Anal. At. Spectrom*., **1998**, *13*, 697.
17. R. J. Watling, *J. Anal. At. Spectrom*., **1998**, *13*, 927.
18. J. L. Nielsen, A. Abildtrup, J. Christensen, P. Watson, A. Cox, and C. W. Mcleod, *Spectrochim. Acta, Part B*, **1998**, *53*, 339.
19. J. J. Leach, L. A. Allen, D. B. Aeschliman, and R. S. Houk, *Anal. Chem*., **1999**, *71*, 440.
20. W. Devos, C. Moor, and P. Lienemann, *J. Anal. At. Spectrom*., **1999**, *14*, 621.
21. B. Wanner, C. Moor, R. Richner, R. Bronnimann, and B. Magyar, *Spectrochim. Acta, Part B*, **1999**, *54*, 289.
22. D. Gunter, S. E. Jackson, and H. P. Longerich, *Spectrochim. Acta, Part B*, **1999**, *54*, 381.
23. A. M. Leach and G. M. Hieftje, *J. Anal. At. Spectrom*., **2000**, *15*, 1121.
24. B. Hattendorf and D. Gunter, *J. Anal. At. Spectrom*., **2000**, *15*, 1125.
25. L. Kempenaers, N. H. Bings, T. E. Jeffries, B. Vekemans, and K. Janssens, *J. Anal. At. Spectrom*., **2001**, *16*, 1006.
26. R. Ma, I. Staton, C. W. Mcleod, M. B. Gomez, M. M.

Gomez, and M. A. Palacios, *J. Anal. At. Spectrom*., **2001**, *16*, 1070.
27. D. Gunther, B. Hattendorf, and A. Audetat, *J. Anal. At. Spectrom*., **2001**, *16*, 1085.
28. A. Plotnikov, C. Vogt, V. Hoffmann, C. Taschner, and K. Wetzig, *J. Anal. At. Spectrom*., **2001**, *16*, 1290.
29. P. R. D. Mason and A. J. G. Mank, *J. Anal. At. Spectrom*., **2001**, *16*, 1381.